05,11

Formation of magnetic phase diagrams in the $Mn_{1-x}Cr_xNiGe$ system with temperature-separated structural and magnetic phase transitions

© V.I. Valkov[1], I.F. Gribanov[1], E.P. Andreichenko[1], O.E. Kovalev[1], V.I. Mityuk[2]

[1] Galkin Donetsk Institute for Physics and Enginireeng, Donetsk, Russia
[2] Scientific-Practical Materials Research Center of the National Academy of Sciences of Belarus, Minsk, Belarus

E-mail: valkov09@gmail.com

Received August 22, 2023
Revised September 3, 2023
Accepted September 4, 2023

The analysis and modeling of magnetostructural diagrams of the $Mn_{1-x}Cr_xNiGe$ system using an exchange-structural model of interacting parameters of spin and structural orders is carried out. The spin subsystem with a helimagnetic order in the rhombic phase is described in the mean field approximation, and the change in the symmetry of the structural subsystem is taken into account in the approximation of a displaced harmonic oscillator. A qualitative agreement was obtained between the theoretical and experimental features of magnetostructural diagrams under pressure up to 14 kbar.

Keywords: magnetostructural transition, magnetic phase diagrams, helimagnetism, baric features.

DOI: 10.61011/PSS.2023.10.57221.187

1. Introduction

In solid solutions of systems based on MnNiGe [1–3] in a number of cases structural paramagnetic transition of the 1st kind, offset type $PM(P6_3/mmc)-PM(P_{nma})$ from hexagonal (hex) phase c crystalline lattice of type Ni_2In in orthorhombic (orth) phase with crystalline lattice of type TiNiSi separated from low temperature magnetic phase transitions of second kind paramagnetism-ferromagnetism $(PM(P_{nma})-FM(P_{nma}))$ [1], paramagnetism-helimagnetism $(PM(P_{nma})-HM(P_{nma}))$ [2–3] by significant (up to 100 K) temperature interval, Figure 1. The most characteristic feature of the magnetostructural P–T diagrams of these systems is the paradoxical behavior, according to Figure 2 ([4–5]), lines of magnetic phase isostructural and magnetostructural transitions of the order–disorder.

At that, when $T_C(h-h) \equiv T_C(\text{hex}-\text{hex})$ — const (Figure 1, *a*), the increase in dependence of temperatures of isostructural magnetic ordering $T_C(o-o)$, $T_N(o-o)$ with pressure increasing, up to the contact of these lines of 2-nd kind transitions with the lability temperatures T_{t1}, T_{t2} of the hexagonal, orthorhombic phases is a paradox because it contradicts the „pattern" of the occurrence of orthorhombic magnetic order, which can be distinguished from the characteristic temperature dependences of the inverse paramagnetic susceptibility $\chi^{-1}(T)$, Figure 2.

Indeed, from the dependences $\chi^{-1}_{\text{hex}}(T)$ and $\chi^{-1}_{\text{orth}}(T)$ it is clear that the paramagnetic Curie temperatures of the hexagonal (Θ_{hex}) and orthorhombic (Θ_{orth}) phases are close to the temperatures of spontaneous occurrence of magnetic order in the corresponding phases are related as $\Theta_{\text{hex}} \ll \Theta_{\text{orth}}$. It is therefore obvious that the stability of the spontaneous magnetically ordered phase with the orthorhombic crystal structure is determined by the stability of the orthorhombic phase. Therefore, if the stability temperature of the orthorhombic phase decreases with pressure increasing $(\partial T_{t1,2}/\partial P < 0$, Figure 1), then it would be obvious to suppose that the stability of the orthorhombic magnetically ordered phase also decreases. However, according to Figure 1, in the temperature-and-pressure region of 2nd kind transitions $\partial T_{C,N}/\partial P > 0$. This contradiction forms the basis for the paradoxical behavior of the lines of magnetic phase transitions of 2nd kind of P–T-diagram.

At pressures $P > 0.5$ GPa (Figure 1, *a*) and $P > 10$ kbar (Figure 1, *b*) a combination of magnetic and structural transitions occurs. A subsequent increase in pressure leads to the transformation of isostructural transitions of 2nd kind

$$PMorth(P_{nma}) \leftrightarrow FMorth(P_{nma}),\ \text{Figure 1}, a$$

$$PMorth(P_{nma}) \leftrightarrow HMorth(P_{nma}),\ \text{Figure 1}, b$$

to magnetostructural transitions pof 1st kind

$$PMhex(P6_3/mmc) \leftrightarrow FMorth(P_{nma}),$$

$$PMhex(P6_3/mmc) \leftrightarrow HMorth(P_{nma}).$$

This process is accompanied not only by the merging of the lability temperatures of the structural T_{t1}, T_{t2} and

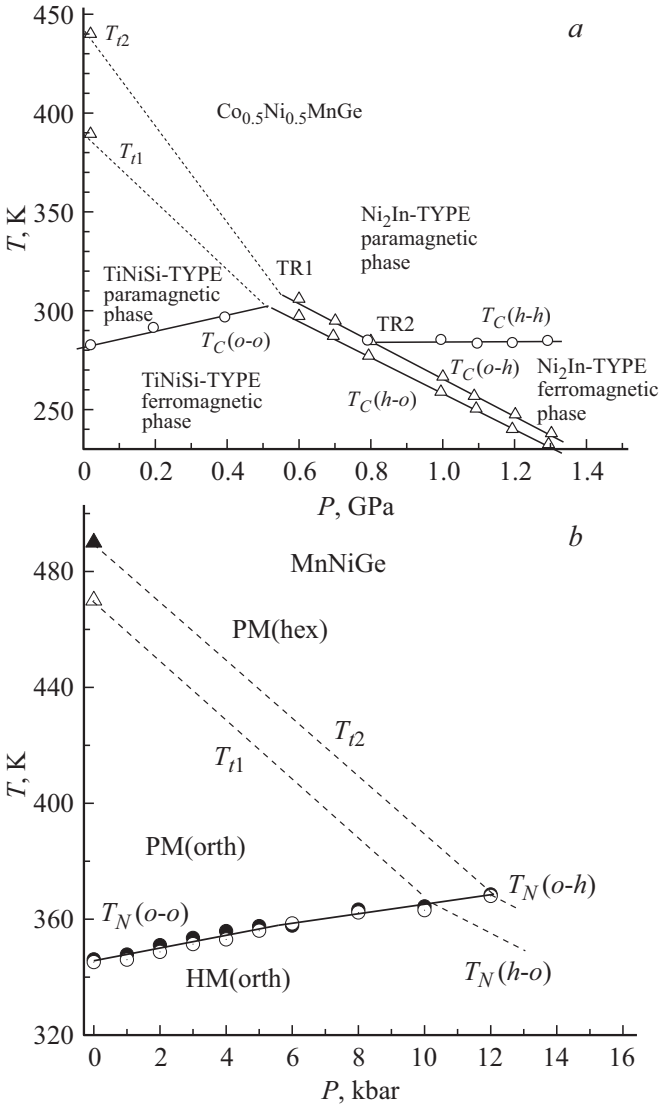

Figure 1. P–T-diagrams $Co_{0.5}Ni_{0.5}MnGe$ (*a*) MnNiGe (*b*) typical For row of Germanides with spaced apart by temperature structural and magnetic phase transitions, *a* — [3], *b* — [2]. $T_{C(N)}(o{-}o)$, $T_N(o{-}o)$ and $T_C(h{-}h)$ — lines of isostructural transitions of 2-nd kind $\mathrm{PMorth}(P_{nma}) \leftrightarrow \mathrm{FM(HM)orth}(P_{nma})$ and $\mathrm{PMhex}(P6_3/mmc) \leftrightarrow \mathrm{FMhex}(P6_3/mmc)$; $T_{C(N)}(o{-}h)$, $T_{C(N)}(h{-}o)$ — corresponding lines of magnetostructural transitions of 1st kind $\mathrm{FM(HM)orth}(P_{nma}) \rightarrow \mathrm{PMhex}(P6_3/mmc)$, $\mathrm{PMhex}(P6_3/mmc) \rightarrow \mathrm{FM(HM)orth}(P_{nma})$.

magnetic $T_{C,N}(o{-}h), T_{C,N}(h{-}o)$ transitions, but also by the disappearance of the abnormal pressure behavior of the orthorhombic magnetically ordered phase: the sign of the pressure derivatives of these quantities changes $(\partial T_{C,N}(o{-}h)/\partial P < 0,\ \partial T_{C,N}(h{-}o)/\partial P < 0)$, Figure 1.

It should be also noted that the occurrence of magnetostructural transitions under pressure leads to additional increase in the magnetocaloric effect (MCE). Since the increase in crystal symmetry from orthorhombic to hexagonal, accompanying the spontaneous magnetic disorder $\mathrm{HMorth}(P_{nma}) \rightarrow \mathrm{PMhex}(P6_3/mmc)$, is summed up with the increase in magnetic symmetry and additional increase in the overall entropy of the system. As a consequence, this leads to increase in the MCE absolute value during demagnetization. Therefore, understanding of the mechanisms of temperature-and-pressure features is of significant practical importance.

This paper relates to the analysis and explanation of the abnormal features of the magnetic phase diagrams of $Mn_{1-x}Cr_xNiGe$ system within the framework of the so-called exchange-structural model.

2. Basic positions of exchange-structural model for interacting structural and spin degrees of freedom

We partially proceed from the provisions set out in papers [5–6], where the initial highly symmetric paramagnetic (PM) state at $T \geq T_{t2}$ corresponds to the hexagonal (hex) paramagnetic state $(P6_3/mmc)$. The low-symmetry PM state at $T \leq T_{t1}$, arising as a result of the 1st kind structural transition $\mathrm{PMhex}(P6_3/mmc) \leftrightarrow \mathrm{Morth}(P_{nma})$, is characterized by the structural order parameter Q_0. According to [5] Q_0 is the average statistical $Q_0 = \langle Q_n \rangle_\rho$ value of the variables Q_n (Appendix). The variables $Q_n = (U_{nz}^{\mathrm{Ni}_1} - U_{nz}^{\mathrm{Ni}_2})/c_{\mathrm{hex}}$ describe V classical approaching local group offsets of atoms Ni_1, Ni_2 in *n*-th hexagonal cell along direction *z*, Figure 3. The appearance of average $Q_0 = \langle Q_n \rangle_\rho$ as inter-cell correlations between local offsets Q_n arises as a result of competition between the intra-cell single-particle potential $W(Q_n) = \sum_n \left(\tilde{\omega}^2 Q_n^2 + \tilde{\gamma} Q_n^4 + \tilde{\Gamma} Q_n^6\right)$ and inter-cell multiparticle interactions $\left(-\sum_{n,n'} V(n,n') Q_n Q_{n'}\right)$ (Appendix). At that it is believed that non-local (common with neighboring cells) offsets of atoms Mn_1 (Mn_2) — $U_{nx}^{\mathrm{Mn}_1}(U_{nx}^{\mathrm{Mn}_2})$ arise due to orthogonal local (belonging to one *n*-th cell) offsets of atoms Ni $U_{nz}^{\mathrm{Ni}_1}$, $(U_{nz}^{\mathrm{Ni}_2})$ and Ge $U_{nx}^{\mathrm{Ge}_1}$, $(U_{nx}^{\mathrm{Ge}_2})$. In general, the group offsets of all atoms of the cell can characterize the amplitude of the phonon soft mode, the freezing of which leads to decrease in the hexagonal symmetry $P6_3/mmc$ to the orthorhombic $Pnma$ and the occurrence of a cooperative structural transition $P6_3/mmc{-}Pnma$ in the entire system.

According to experimental data [7–8] the magnetically ordered state with orthorhombic system (orth) corresponds to simple helimagnetic structure described by the wave vector $\mathbf{q} = [0, 0, q_a]$. As a magnetic order parameter we consider the variable $y = \langle \mathbf{U}_n^k \hat{\mathbf{s}}_n^k \rangle / s = \langle \hat{m}_n^k \rangle / s \equiv m/s$, which in the framework of the Heisenberg model in the mean field approximation (MFA) is defined (Appendix) as the statistical average $\langle \hat{m}_n^k \rangle \equiv m$ of the projection of the operator $\hat{m}_n^k$ of that *k*-atom spin (Mn) $\hat{\mathbf{s}}_n^k$ in *n*-th hexagonal cell to the direction of the local quantization axis $\mathbf{U}_n^k$ [6].

In the original papers [5–6] the relationship between the spin and structural subsystems was determined by the presence in the components J_i of the Fourier components

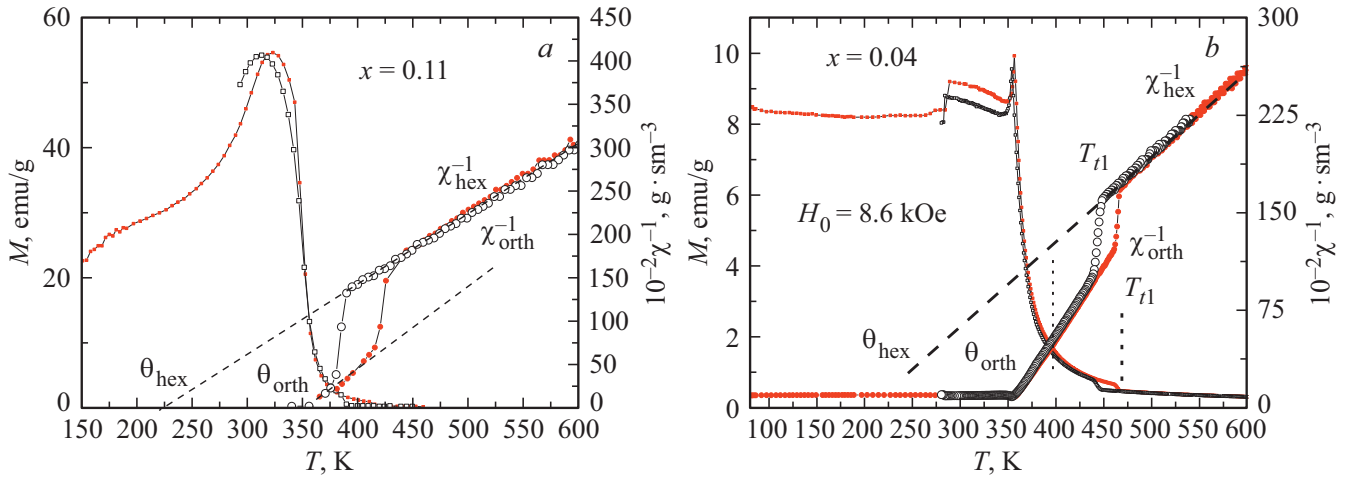

Figure 2. Characteristic temperature dependencies of magnetization σ and reverse susceptibility χ^{-1} of samples of system $Mn_{1-x}Cr_xNiGe$, [4-5].

of interatomic exchange interactions (1) of combinations of structural order parameters Q_n^2 with elastic deformations of the type $e_1Q_0^2$.

$$J(q_a) = \sum_{\mathbf{\Delta R}} J(|\mathbf{\Delta R}_{nn'}^{kk'}|)\cos(\mathbf{q}\mathbf{\Delta R}_{nn'}^{kk'})$$

$$\approx \sum_{i=0}^{2} J_i(Q_0^2, e_1Q_0^2)\cos(i\Psi), \qquad (1a)$$

$$J_i = \sum_{\mathbf{\Delta R}_{i=0}}^{2} J(|\mathbf{\Delta R}_i|), \qquad (1b)$$

where $\mathbf{\Delta R}_i = [\Delta R_x, \Delta R_y, ic_{\text{hex}}/2]$; J_i — corresponding components Fourier components of integrals of exchange interactions inside ferromagnetic layer and between closest layers at distances $|\mathbf{\Delta R}_1| = c_{\text{hex}}/2$ and $|\mathbf{\Delta R}_2| = c_{\text{hex}}$, $\Psi = \mathbf{q}_a c_{\text{hex}}/2$, $2\Psi = \mathbf{q}_a c_{\text{hex}}$, with accounting of nearest neighbors in hexagonal basic plane $\sqrt{(\Delta R_x)^2 + (\Delta R_y)^2} = a_{\text{hex}}$ where c_{hex} and a_{hex} — parameters of hexagonal lattice along and perpendicular the direction z.

At the same time, in papers [5–6] the appearance of the dependences $J_i(Q_0^2, e_1Q_0^2)$ as a limited response of the spin subsystem to the offset of Ni atoms was accepted a priori. This approach made it possible to describe the increase in magnetic disorder temperatures ($\partial T_{N,C}/\partial P > 0$) in the region of isostructural transitions of 2nd kind, $\text{PM}(P_{nma})-\text{HM}(P_{nma})$, at low pressures about $P < 7$ kbar, and the transformation of these transitions to 1st kind magnetostructural transitions at high pressures. However, the persistence of an increase in the dependences $T_{N_{1,2}}(P)$, coinciding with the lability temperatures of first-order magnetostructural transitions $\text{PM}(P6_3/mmc) \leftrightarrow \text{HM}(P_{nma})$, determines the qualitative discrepancy between theoretical and experimental (Figure 1) P–T-diagrams, in which such

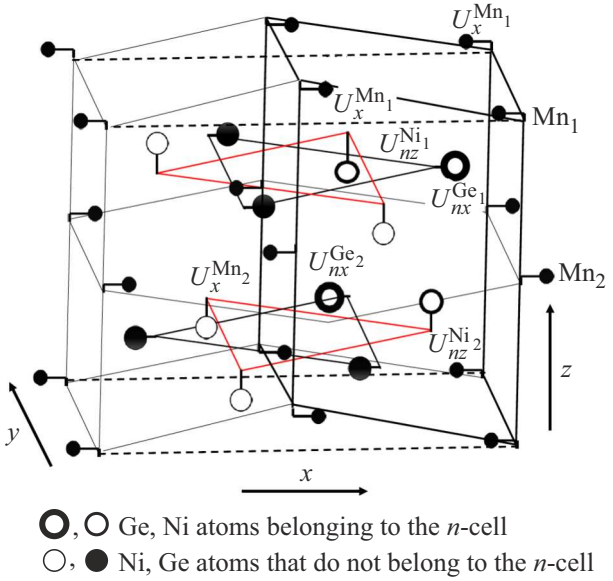

Figure 3. Local optical displacements $U_{nz}^{Ni_1}$, $(U_{nz}^{Ni_2})$, $U_{nx}^{Ge_1}$, $(T_{nx}^{Ge_2})$ of Ni and Ge atoms, respectively, related to n-th hexagonal cell of MnNiGe type Ni_2In (shown by bold lines). The dashed lines highlight the base region of the orthorhombic cell of the MnNiGe type.

dependences undergo a break and become decreasing functions of pressure.

In this paper, we proceed from the fact that the coupling between the spin and structural subsystems should be described by competing contributions. One of them can be obtained by taking into account the response of the structural (phonon) subsystem to a change in the degree of polarization of the bonding and antibonding electronic d-states of magnetically active atoms. In the approach under consideration, which uses the Heisenberg form to describe interactions in the spin subsystem, the Hamiltonian of the

structure-spin interaction can be represented in the form

$$\hat{\mathbf{H}}_{sQ} = -\sum_{nk,n'k'} (L_{nn'}^{kk'}\hat{\mathbf{s}}_n^k\hat{\mathbf{s}}_{n'}^{k'}Q_nQ_{n'} + e_1 l_{nn'}^{kk'}\hat{s}_n^k\hat{\mathbf{s}}_{n'}^{k'}Q_nQ_{n'})$$

$$\approx -\sum_{nk,n'k'} (L_{nn'}^{kk'} + e_1 l_{nn'}^{kk'})\hat{\mathbf{s}}_n^k\hat{\mathbf{s}}_{n'}^{k'}\langle Q_nQ_{n'}\rangle_\rho$$

$$-\sum_{nk,n'k'} (L_{nn'}^{kk'} + e_1 l_{nn'}^{kk'})\langle\hat{\mathbf{s}}_n^k\hat{\mathbf{s}}_{n'}^{k'}\rangle_h Q_nQ_{n'}. \quad (2)$$

In this case, according to (A15b) of the Appendix, the components $J(q_a)$ and j_i are transformed into the components $\tilde{J}(q_a)$ and $\tilde{J}_i(Q_0)$, which are expressed through

$$\sum_{nk,n'k'} L_{nn'}^{kk'}\langle Q_nQ_{n'}\rangle_\rho$$

and are as follows

$$\tilde{J}(q_a) \approx \sum_{i=0}^{2} \tilde{J}_i(Q_0^2, e_1Q_0^2)\cos(i\Psi), \quad (3a)$$

$$\tilde{J}_i(Q_0) = \sum_{\Delta\mathbf{R}_i}\Big[J(|\Delta\mathbf{R}_i|) + \big[2L(|\Delta\mathbf{R}_i|) + e_1 2l(|\Delta\mathbf{R}_i|)\big]Q_0^2\Big]$$

$$= J_i + [2L_i + e_1 2l_i]Q_0^2. \quad (3b)$$

This contribution is identical in form to (1) and retains all its shortcomings. The second competing contribution can arise if we directly take into account the changes in the Fourier components of the exchange interaction J_i upon offset of Ni atoms. The appearance of the competing contribution may be a consequence of more complex changes in the variable $\tilde{J}(q_a)$ accompanying the structural transition. Indeed, it is logical to assume that in the system under study, interatomic exchange interactions are formed in the form of superposition of indirect and kinetic exchanges [9] and significantly depend on the overlap and distortion of the wave functions of d-electrons. It can be assumed that changes in overlap caused by the breaching of the hexagonal crystal system form the dependence $J_i \equiv J_i(Q_0)$, which is qualitatively different from $[2L_i + e_1 2l_i]Q_0^2$.

Expressions for the complete TP of the system $\Omega = \tilde{\Omega}_s + \tilde{\Omega}_Q + \Omega_e$ taking into account (3) are given in the Appendix (Ω_e — TP of the elastic subsystem with hexagonal symmetry [10]).

Equilibrium dependences of magnetic, structural and elastic characteristics can be obtained from the equations

$$\partial J(q_q)/\partial\Psi = 0, \quad \partial\Omega/\partial\vartheta = 0, \quad \partial\Omega/\partial\tilde{\sigma} = 0,$$

$$\partial\Omega/\partial e_1 = 0, \quad \partial\Omega/\partial e_2 = 0, \quad (4)$$

$$\partial\Omega/\partial y = 0, \quad \partial\Omega/\partial Q_0 = 0, \quad (5)$$

$e_1 = e_{xx} + e_{yy} + e_{zz}$ and $e_2 = (e_{xx} - e_{yy})/\sqrt{3} \neq 0$ elastic volumetric and orthorhombic deformations of the cell as a whole. Equations $\partial J(q_a)/\partial\Psi = 0$, $\partial\Omega/\partial\vartheta = 0$, allow us to obtain conditions for the existence of helimagnetic structure without field (A14) and in field at $\mathbf{H}_0 = [0, 0, H_0]$, $H_0 > 0$ (P21).

When specifying a specific approximation of the dependence $J_i \equiv J_i(Q_0)$, the next three equations have analytical solutions in the form of dependencies: $e_1 = e_1(y, Q_0, T, P)$, $e_2 = e_2(Q_0)$, $\tilde{\sigma} = \tilde{\sigma}(Q_0, T)$. The last two equations (5) $\partial\Omega/\partial Q_0 = 0$, $\partial\Omega/\partial y = 0$ are reduced to the form (6) and solved numerically

$$(\partial\Omega/\partial Q_0) = 0, \quad (6a)$$

$$y = B_s(X), \quad (6b)$$

$$B_s(X) = \left[\left(\frac{1}{2s+1}\right)\coth\frac{1}{2s+1}X - \left(\frac{1}{2s}\right)\coth\frac{1}{2s}X\right]$$

— Brillouin function $X = hs/k_BT$.

The solutions of the system of equations (6) determine the behavior of the temperature dependences of the magnetostructural characteristics of the model under study. This parameters of structural $Q_0(T)$ and magnetic $y(T)$ orders ; magnetization $\sigma(T)$ for given values of magnetic field strengths H_0 (7a) and dimensionless reverse paramagnetic susceptibility $\chi^{-1}(T)$ in the limit $H_0 \to 0$ (7b).

$$\sigma(T) = M_0(x)y(T)\cos\vartheta(T), \quad (7a)$$

$$\chi^{-1}(T) = \frac{T}{T_0} - h_{Fm}(T), \quad (7b)$$

$$h_{Fm}(T) = h_m(q_a = 0, y = 0),$$

$M_0(x)$ — maximum magnetic moment at collinear configurations $(\cos\vartheta(T) = 1)$ of localized spins Mn for sample with given number x and spin $s = 3/2$; for his calculation we use expression

$$M_0\,[\text{emu/g}] = (1-x)2s\mu_B/A(x)$$

$$= 1.116906^* s^* 10\,000^*(1-x)/A, \quad (8)$$

$A(x)$ — atomic weight per formula unit.

Further analysis of solutions (6) showed that the convergence of theoretical and experimental P–T-diagrams is achieved if the dependencies $J_i(Q_0)$, $\tilde{J}(q_a)$ are represented in the form (9), (10) at $1/2 < d < 1$. In this case, competition between the initial contributions $L_iQ_0^2$ and contributions from $J_i(Q_0)$ can lead to a change in sign of $\partial T_{C_{1,2}}(P)/\partial P$, $\partial T_{N_{1,2}}(P)/\partial P$ at high pressures.

$$J_i(Q_0) = J_{i0} + |Q_0|^{2d}\{\lambda_{i0} + \lambda_{i1}e_1 + \lambda_{i4}|Q_0|^{2d}\}, \quad (9)$$

$$\tilde{J}(q_a) \approx \sum_{i=0}^{2}\tilde{J}_i(Q_0)\cos(i\Psi)$$

$$\equiv \sum_{i=0}^{2} J_i(Q_0)\cos(i\Psi) + \sum_{i=0}^{2} 2L_i(Q_0)\cos(i\Psi)$$

$$\equiv J_{00}\Big[r_{AF} + |Q|_0^{2d}(\lambda_{AF} + \lambda_{1AF}e_1)^2 + 2\lambda|Q|_0^{4d}\Big] + J_{00}2L_{AF}Q_0^2, \quad (10)$$

Table 1. Basic experimental data and their changes under pressure for the $Mn_{1-x}Cr_xNiGe$ system

$x\downarrow$	T_{t2}	T_{t1}	$\cos\psi$	$\frac{\sigma_m(0)}{\sigma_m(12)}$	$\left(\frac{\partial T_N}{\partial P}\right)_0$	$\left(\frac{\partial T_{N_2}}{\partial P}\right)_{12}$	θ_{hex}	θ_{orth}
Unit of meas. $\rightarrow$	K			emu/g	K/kbar		K	
0.11	431	390	0.92−0.9	$\frac{49.9}{51.2}$	3.05	−4.6	225	350
0.07	449	423		$\frac{28}{49}$	2.5	−1.4		
0.04	460	443	0.8−0.87	$\frac{10.5}{27.5}$	2.7	−5.7	225	350

Table 2. Main reference constants of thermodynamic potential used to describe the baric features of magnetostructural characteristics

$x\downarrow$	ν_0	A	B	δ	λ_{00}	λ_{20}	$M_0(x)$	$-L_{20}$	$-\lambda_{01}$	$\frac{a_3}{10^{-5}}$	T_0
Unit of meas. $\rightarrow$	kbar						emu/g			kbar	K
0.11	43.616	9	98	0.918	27.2	1.646	80.2	2.68	141.9	307	50
0.07	44/137	11.8	98	0.827	28	2.02	83.75	10.56	141.9	321	50
0.04	44.544	18	08	0.724	34.4	1.197	86.4	12.32	141.9	331	49

Note. The values $a_3 = Nk_B$ are calculated based on X-ray density values. The values $M_0(x)$ are calculated for spin $s = 3/2$ by formula (8), $L_{00} = \lambda_{21} = 0$.

$$r_{AF} = 1 + K(\Psi, Q_0), \quad \lambda_{AF} = \lambda_{00} + \lambda_{20}K(\Psi, Q_0),$$
$$\lambda_{1AF} = \lambda_{01} + \lambda_{21}K(\Psi, Q_0), \tag{11a}$$
$$\lambda_{4AF} = \lambda_{04} + \lambda_{24}K(\Psi, Q_0), \quad L_{AF} = L_{00} + L_{20}K(\Psi, Q_0),$$
$$\delta(Q_0) = 1 - AQ_0^2 + BQ_0^4, \tag{11b}$$
$$J_{00} = J_0(Q_0 = e_1 = 0) = k_B T_0\, 2/3s(s+1),$$
$$K(\Psi, Q_0) = \frac{J_{20}}{J_{00}}\left(\cos(\Psi) - 1\right)\left[2\delta(Q_0) - \cos(\Psi) - 1\right]. \tag{11c}$$

The values of the constants in (11) are given in Tables 1, 2.

3. Results of numerical solutions of equations of state for specific systems $Mn_{1-x}Cr_xNiGe$ with given concentration x

When choosing the values of the constants (Table 2), a number of experimental data at atmospheric pressure were used (Table 1). Which include parameters of helicoidal structure $\cos(\Psi)$, maximum values of magnetization $\sigma_m(0)$, $\sigma_m(12)$ in field $H_0 = 9.7$ kOe and pressures $P = 0$, $P = 12$ kbar, values of temperatures of magnetic $T_N(x)$ and structural $T_{t1,2}(x)$ transitions and their derivatives $(\partial T_N/\partial P)_0$, $(\partial T_{tN2}/\partial P)_{12}$ at $P = 0$ and $P = 12$ kbar, values paramagnetic Curie temperatures $\theta_{\text{hex}}(x)$, $\theta_{\text{orth}}(x)$.

Verification of theoretical results for samples of $Mn_{1-x}Cr_xNiGe$ system was considered satisfactory if a once-made choice of constants with reference to experimental data for atmospheric pressure allowed a qualitatively correct description of their changes for arbitrary pressures (Table 1).

For example, the comparison was made of the isobaric experimental and theoretical dependences of the inverse paramagnetic susceptibility $\chi^{-1}(T)$ and magnetization $\sigma(T) = y(T)M_0(x)\cos[\vartheta(T)]$ in the pressure range 0−12 kbar and magnetic fields up to $H_0 = 9.7$ kOe, Figure 4, 5.

In Figure 4 the peripheral high-temperature jumps in magnetization $\Delta_{1,2}\sigma$ illustrate the magnetostructural mechanism of the abnormal behavior in the PM region of 1st kind $\text{hex}(P6_3/mmc) \leftrightarrow \text{orth}(P_{nma})$; Figure 2. Link of jumpers of $\Delta_{1,2}\sigma = H_0/\chi^{-1}(T)$ with jumpers of structural order parameter Q_0 during the structural transition is traced from Figure 4, *b, d, f.* The appearance of magnetization maximum with temperature decreasing in Figure 4 correlates with the experimental graphs (Figure 2) and arises as a result of competition between two contributions to the average field (A16). Exchange spatially periodic contribution $2s\,y\left[\tilde{J}(q_a)\sin^2(\vartheta) + \tilde{J}(0)\cos^2(\vartheta)\right]$ and spatially homogeneous contribution from the external magnetic field $2\mu_0 H_0\cos(\vartheta)$. In this case, at temperatures $T_m < T \le T_N$ when $y(T) \ll 1$ in finite field H_0 according to (A21) $\cos(\vartheta) = 1$, and increase in the magnetic order parameter with temperature decreasing, according to (6b), it results in increase in magnetization $\sigma(T) = M_0(x)y(T)\cos\vartheta(T)$. At temperatures $T \le T_m$, if the condition (A21) occurs, $\cos\vartheta(T)$ deviates from 1 and, according to calculations, rapidly decreases in value, which makes it obvious that maximum can be realized in the temperature dependence $\sigma(T) = M_0(x)y(T)\cos\vartheta(T)$.

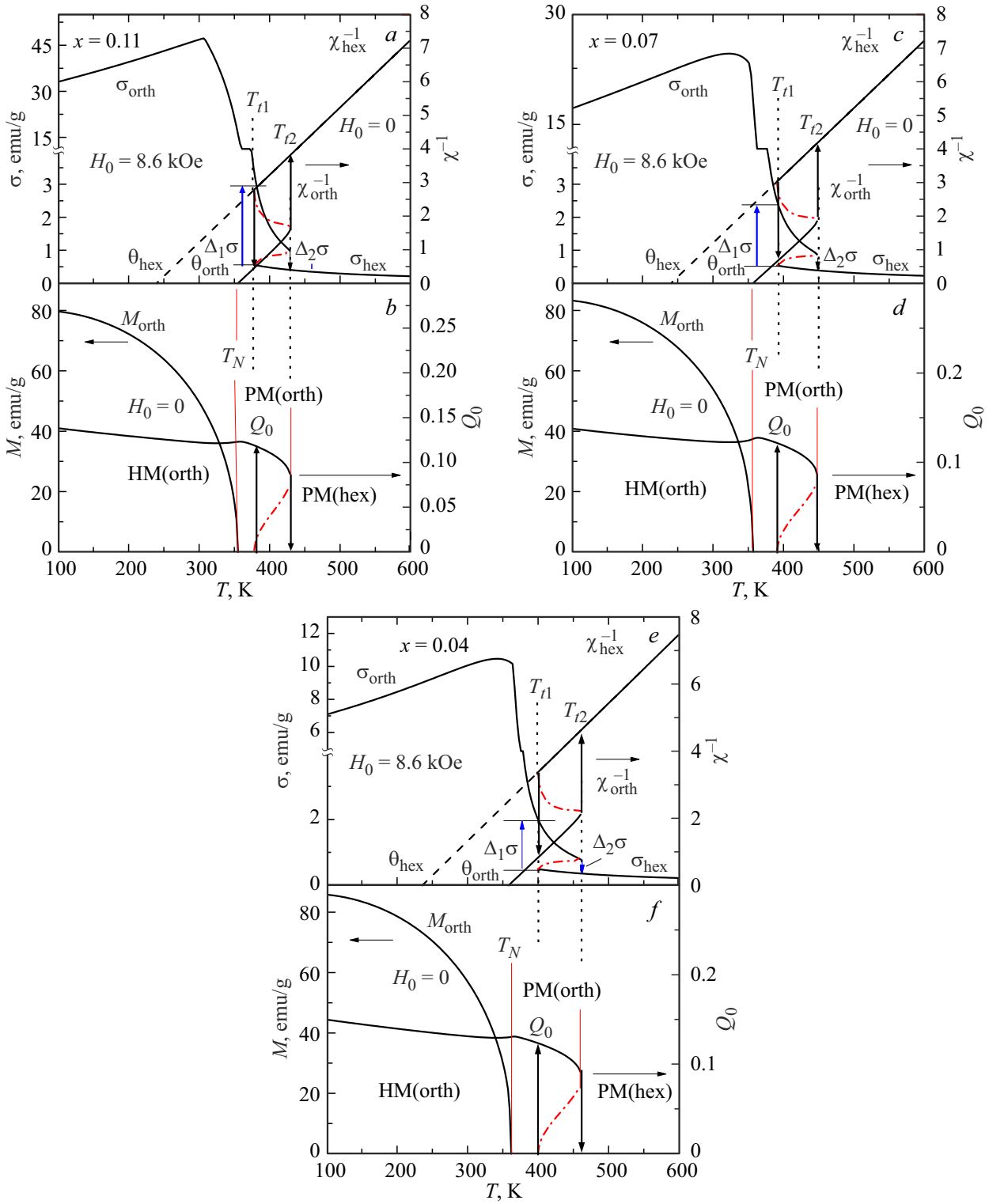

Figure 4. Theoretical temperature dependences of magnetostructural characteristics compared to samples of $Mn_{1-x}Cr_xNiGe$ system at atmospheric pressure. The magnetization $\sigma(T) = M_0(x)y(T)\cos\vartheta(T)$ and the dimensionless structural order parameter $Q_0(T)$ were calculated in the field $H_0 = 8.6$ kOe; spin magnetic moment of manganese atoms $M(T) = y(T)M_0(x)$ in units of emu/g, dimensionless inverse paramagnetic susceptibility $\chi^{-1}(T)$ calculated in the field $H_0 = 0$; dash-dot lines — describe the metastable sections of the corresponding dependencies.

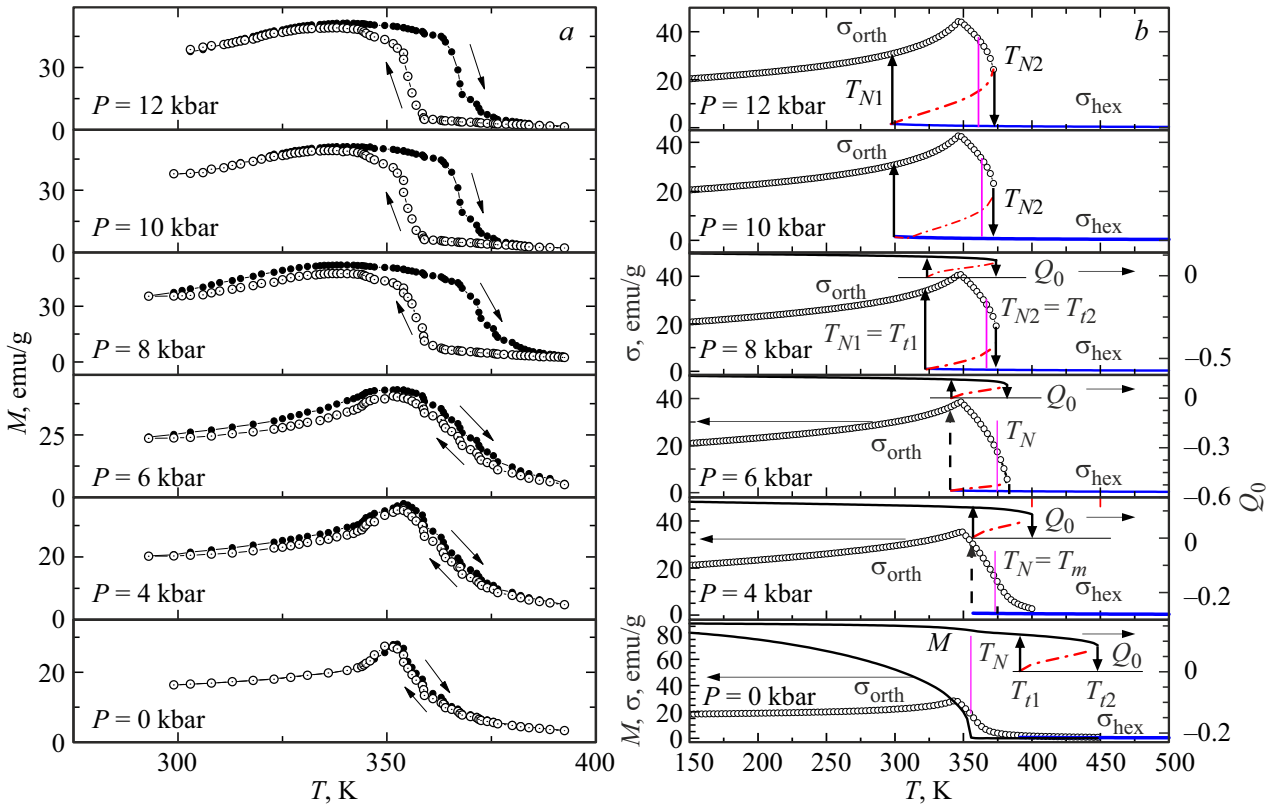

Figure 5. Comparison of isobaric experimental (left) and theoretical (right) temperature dependences of magnetization σ of sample $Mn_{0.83}Cr_{0.07}NiGe$ in external magnetic field $H_0 = 9.7$ kOe. The dependence $M(T) = y(T)M_0(x)$ was calculated at $H_0 = 0$ to determine the spontaneous Néel temperature T_N in P–T region of 2nd kind transitions.

The main effects of hydrostatic pressure action on samples of $Mn_{1-x}Cr_xNiGe$ system with magnetic and structural transitions separated by temperature can be traced in Figure 5. The most significant among them is the change in the nature of magnetic ordering from isostructural transitions of 2nd kind $PM(P_{nma}) - HM(P_{nma})$ at relatively low pressures to magnetostructural transitions of 1st kind $PM(P6)3/mmc) \leftrightarrow HM(P_{nma})$ at pressures about 8 kbar and higher.

The mechanism of pressure transformation of magnetic ordering is due to the combination of temperatures of magnetic and structural transitions. This is clear from Figure 5, *b*, where convergence and combination of dependences of magnetic σ, y and structural Q_0 characteristics upon pressure increasing to 8 bar leads to the disappearance of smooth magnetic phase transitions within the orthorhombic symmetry $(Q_0 \neq 0)$ and the appearance of jump-like magnetostructural transitions, accompanied by change in symmetry $PM(P6_3/mmc - Q_0 = 0) \leftrightarrow HM(P_{nma} - Q_0 \neq 0)$. In this case, the transformation of the transitions is accompanied not only by the appearance of temperature hysteresis, but also by characteristic jump-like magnetostructural deformation of the lattice cell (Figure 6, *c, d*), which may be the cause of the virgin effect, studied in [11]. At atmospheric pressure the jump-like change in these variables is observed only in the region of PM structural transition, Figure 6, *a, b*. This result reflects the fact of superposition of magnetic and structural deformation contributions for 1st kind magnetostructural transitions $PM(P6_3/mmc) \leftrightarrow HM(P_{nma})$ at $P = 12$ kbar. A similar superposition of entropy contributions is observed for the magnetocaloric effect when calculating the pressure effects of enhancing the change in isothermal entropy $\Delta 1S = S^{H_0}_{1orth} - S^{0}_{1hex} \gg S^{H_0}_{1orht} - S^{0}_{1orth}$ [12].

Another important feature of the dependences $\sigma(T)$ accompanying the increase in pressure is significant increase in magnetization (by almost two times). This effect can be interpreted as decrease in the spatially inhomogeneous contribution to the exchange field due to the baric instability of the orthorhombic structure.

Also note that the above features arise due to baric convergence and combination of structural and magnetic transitions. When decrease in the temperature of the structural transition occurs with the increase in the Néel temperature of the magnetic transition. As we noted, this may be a consequence of the competition of opposite tendencies in the stabilization of the magnetically ordered phase at side of the spin and phonon subsystems. Therefore, it is of significant interest to analyze the comparison of experimental (Figure 7, *d, e, f*) and calculated (Figure 7, *a, b, c*)

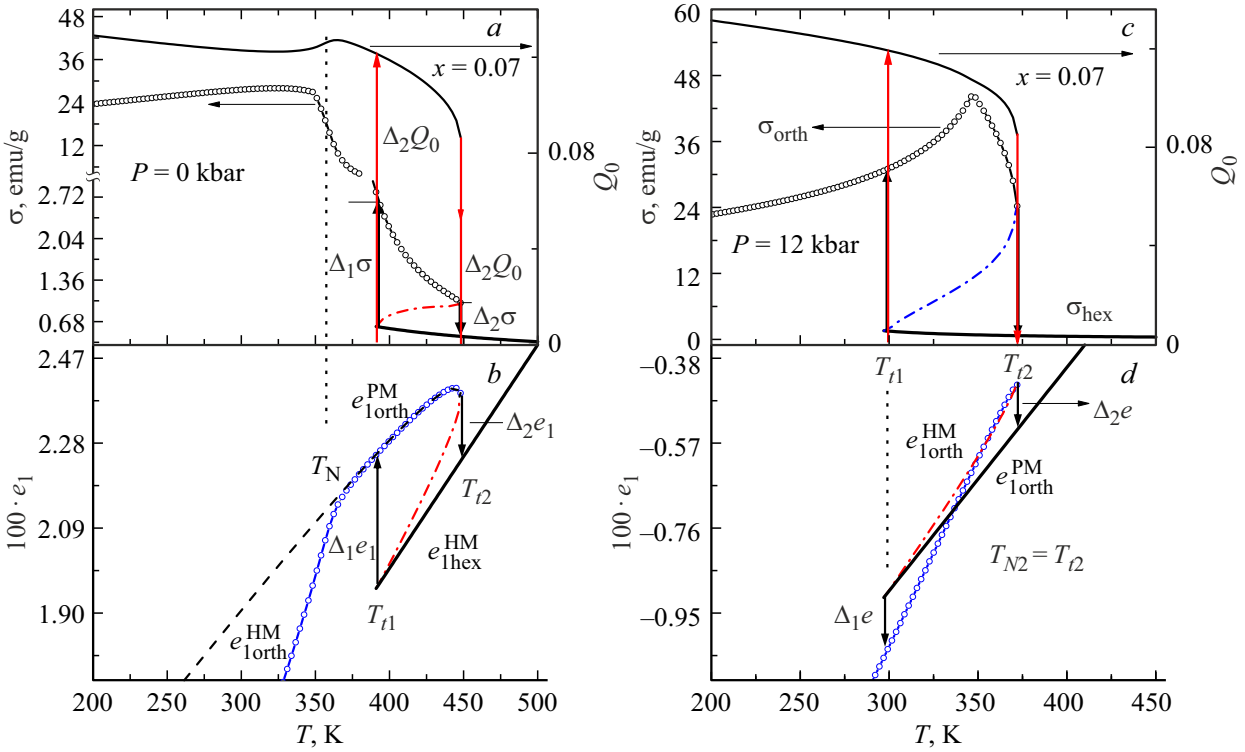

Figure 6. Change in magnetostructural characteristics with pressure increasing.

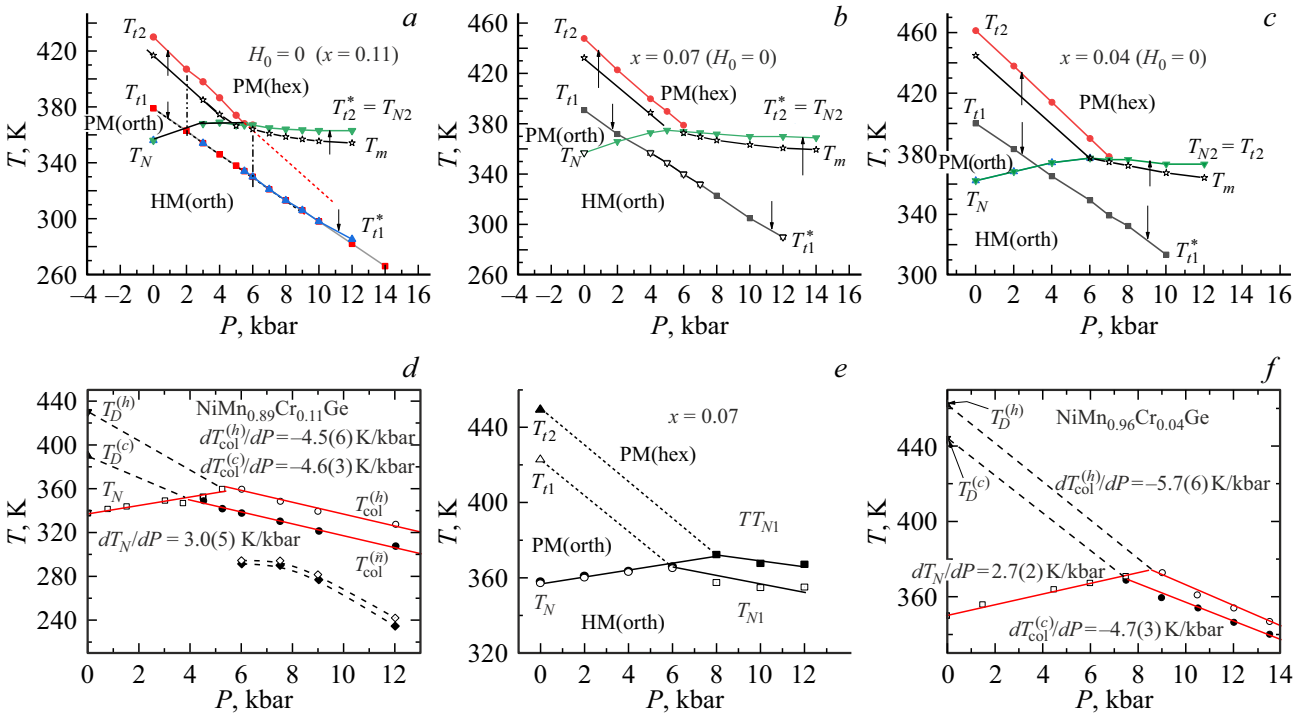

Figure 7. mparison of theoretical (a, b, c) and experimental (d, e, f) [8] P–T-diagrams of alloys of $Mn_{1-x}Cr_xNiGe$ system. ↓, ↑ indicate the lability temperatures of hex$(P6_3/mmc)$, orth(P_{nma}) phases with decrease, increase in temperatures at $T = T_m$. $\Omega(|Q_0| > 0, |y| \geq 0) = \Omega(|Q_0| = 0, |y| = 0)$.

of magnetic phase P–T diagrams for 3 samples of the system under study.

Magnetostructural transitions of 1st kind from the helimagnetic orthorhombic phase to the paramagnetic hexagonal phase $\mathrm{HM}(P_{nma}) \rightarrow \mathrm{PM}(P6_3/mmc)$, accompanied, according to Figure 6, by striction phenomena, occur at the lability temperature $T = T_{t2} \equiv T_{N2}$. The reverse transition $\mathrm{PM}(P6_3/mmc) \rightarrow \mathrm{HM}(P_{nma})$, accompanied by increase in the volume of the lattice cell, depending on the microstructure of samples, can be realized in the interval $T_{t1} \leq T_{N1} \leq T_m$. Comparison with experimental P–T diagrams indicates that the actual P–T boundaries of stability loss of the hexagonal state T_{t1} and T_{N1} are closer to the line T_m.

4. Conclusion

In the exchange-structural model under consideration, in the approximation of an ideal single-domain crystal, it was possible to reflect at a qualitative level the most important baric features of the observed magnetostructural and magnetovolume characteristics, which include the following.

Baric transformation of isostructural transitions of 2nd kind to magnetostructural transitions of 1st kind.

The increase in the magnetic field-induced magnetization of the helimagnetic state with pressure increasing.

Opposite tendencies of stabilization of the magnetically ordered phase in P–T region of existence of transitions of 1st and 2nd kind.

Funding

The study was performed under the state assignment.

Conflict of interest

The authors declare that they have no conflict of interest.

Appendix

$$\hat{\mathbf{H}}_s = -\sum_{nk,n'k'} J_{nn'}^{kk'} \hat{\mathbf{s}}_n^k \hat{\mathbf{s}}_{n'}^{k'} - 2\mu_0 \mathbf{H}_0 \sum_{nk} \hat{\mathbf{s}}_n^k, \qquad (\Pi 1)$$

$$\hat{\mathbf{H}}_{sQ} = -\sum_{nk,n'k'} L_{nn'}^{kk'} \hat{\mathbf{s}}_n^k \hat{\mathbf{s}}_{n'}^{k'} Q_n Q_{n'}, \qquad (\Pi 2)$$

$$H_Q = \sum_n \left(\frac{1}{2}\omega^2 Q_n^2 + \frac{1}{4}\gamma Q_n^4 + \frac{1}{6}\Gamma Q_n^6 \right) - \frac{1}{2}\sum_{n,n'} V(n,n') Q_n Q_{n'}. \qquad (\Pi 3)$$

The complete TP of the system Ω is determined by superposition

$$\Omega = \tilde{\Omega}_s + \tilde{\Omega}_Q + \Omega_e, \qquad (\Pi 4)$$

$$\tilde{\Omega}_s = \langle \tilde{\hat{\mathbf{H}}}_s - \hat{\mathbf{H}}_{hs} \rangle_h - Nk_\mathrm{B}T \ln[z(X)], \qquad (\Pi 5)$$

$$\tilde{\Omega}_Q = \langle \tilde{H}_Q \rangle_\rho - TS(\rho), \qquad (\Pi 6)$$

where for the TP of the elastic subsystem a simplified version is used

$$\Omega_e = \frac{1}{2} e_1^2/\kappa_1 + \frac{1}{2}(e_2)^2/\kappa_2 + Pe_1 - T\alpha e_1/\kappa_1 \ [10];$$

$\alpha, \kappa_1, \kappa_2$ — coefficients of volumetric thermal expansion, volumetric compressibility and elastic constant, respectively

$$\hat{\mathbf{H}}_{hs} = -\sum_{nk} h\mathbf{U}_n^k \hat{\mathbf{s}}_n^k = -\sum_{nk} h\hat{m}_n^k = Nh\hat{m}, \qquad (\Pi 7)$$

$$\tilde{\hat{\mathbf{H}}}_s = -\sum_{nk,n'k'} \left(J_{nn'}^{kk'} + L_{nn'}^{kk'} \langle Q_n Q_{n'} \rangle_\rho \right) \hat{\mathbf{s}}_n^k \hat{\mathbf{s}}_{n'}^{k'} - 2\mu_0 \mathbf{H}_0 \sum_{nk} \hat{\mathbf{s}}_n^k, \qquad (\Pi 8)$$

where $\hat{\mathbf{s}}_n^k (\hat{\mathbf{s}}_{n'}^{k'})$ — operators spins $k(k')$ atoms in $n(n')$ hexagonal lattice cells; $|\mathbf{U}_n^k| = 1$, $\hat{m}_n^k = U_n^k \hat{\mathbf{s}}_n^k$ — operator of spin projections on axis of quantization,

$$\tilde{H}_Q = \sum_n \left(\frac{1}{2}\omega^2 Q_n^2 + \frac{1}{4}\gamma Q_n^4 + \frac{1}{6}\Gamma Q_n^6 \right) - \frac{1}{2}\sum_{n,n'} \left(V(n,n') + 2\sum_{k,k'} L_{nn'}^{kk'} \langle \hat{\mathbf{s}}_n^k \hat{\mathbf{s}}_{n'}^{k'} \rangle_h \right) Q_n Q_{n'}, \qquad (\Pi 9)$$

$$\tilde{\Omega}_s + \tilde{\Omega}_Q = \sum_{nk,n'k'} \left(J_{nn'}^{kk'} + 2L_{nn'}^{kk'} \langle Q_n Q_{n'} \rangle_\rho \right) \langle \hat{\mathbf{s}}_n^k \hat{\mathbf{s}}_{n'}^{k'} \rangle_h - 2\mu_0 \mathbf{H}_0 \sum_{nk} \langle \hat{\mathbf{s}}_n^k \rangle_h + Nh\langle \hat{m} \rangle_h - Nk_\mathrm{B}T \ln[z(X)] + \sum_n \left(\frac{1}{2}\tilde{\omega}^2 \langle Q_n^2 \rangle_\rho + \frac{1}{4}\tilde{\gamma} \langle Q_n^4 \rangle_\rho + \frac{1}{6}\tilde{\Gamma} \langle Q_n^6 \rangle_\rho \right) - \frac{1}{2}\sum_{n,n'} \left(V(n,n') \right) \langle Q_n Q_{n'} \rangle_\rho - TS(\rho). \qquad (\Pi 10)$$

In (A5)–(A10) averaging in MFA

$$\langle A(\hat{m}) \rangle_h = Sp\, A(\hat{m}) e^{\beta h \hat{m}} / z(X);$$

For averaging

$$\langle B(Q_n) \rangle_\rho = \int_{-\infty}^{\infty} \rho_{\mathrm{dso}}\, B(Q_n) dQ_n$$

the single-particle probability density $\rho_{\mathrm{dso}}(Q_n)$ is used for biased harmonic oscillator [13].

$$z(X) = Sp\, e^{\beta h \hat{m}} \equiv \sum_{m_s=-s}^{s} e^{\beta h m_s}; \quad X = hs/k_\mathrm{B}T, \qquad (\Pi 11)$$

$$ys = \langle \hat{m} \rangle = Sp\, \hat{m} e^{\beta h \hat{m}} / z(X), \qquad (\Pi 12a)$$

$$\rho_{\mathrm{dso}} \equiv \rho_{\mathrm{dso}}(Q_n) = \frac{1}{\sqrt{2\pi\tilde{\sigma}}} \exp\left[-\frac{(Q_n - Q_0)^2}{2\tilde{\sigma}} \right], \qquad (\Pi 12b)$$

$$\tilde{\sigma} = \langle [Q_n - Q_0]^2 \rangle_\rho; \quad \langle Q_n \rangle_\rho = \int_{-\infty}^{\infty} \rho_{\text{dso}} Q_n dQ_n. \quad (\Pi 12c)$$

In this case, the variables Q_0, $\tilde{\sigma}$ are considered as independent variables. Then at $\mathbf{H}_0\mathbf{U}_n^k = H_0\cos(\vartheta)$; $\langle \tilde{\mathbf{s}}_n^k \rangle_h = \mathbf{U}_n^k \langle \hat{m}_n^k \rangle_h = \mathbf{U}_n^k \langle \hat{m} \rangle_h = \mathbf{U}_n^k y s$ (P10) can be reduced to the form

$$\tilde{\Omega}_s + \tilde{\Omega}_Q = -N\langle \hat{m} \rangle_h^2 \left[\tilde{J}(q_a)\sin^2(\vartheta) + \tilde{J}(0)\cos^2(\vartheta) \right] - N2\mu_0 H_0 \cos(\vartheta)\langle \hat{m} \rangle_h + N\langle \hat{m} \rangle_h h + U(Q_0, \tilde{\sigma}) - TS(\tilde{\sigma}), \quad (\Pi 13a)$$

$$U(Q_0, \tilde{\sigma}) = \frac{\omega^2}{2}(Q_0^2 + \tilde{\sigma}) + \frac{\gamma}{4}(Q_0^4 + 6Q_0^2\tilde{\sigma} + 3\tilde{\sigma}^2) + \frac{\Gamma}{6}(Q_0^6 + 15Q_0^4\tilde{\sigma} + 45Q_0^2\tilde{\sigma} + 15\tilde{\sigma}^3) - \frac{1}{2}\nu_0(1 + L_2e_1 + L_3e_2)Q_0^2, \quad (\Pi 13b)$$

$$S(\tilde{\sigma}) = -k_{\text{B}} \sum_n \langle \ln \rho_{\text{dso}}(Q_n) \rangle = -k_{\text{B}} N_0 \int_{-\infty}^{\infty} \rho_{\text{dso}}(Q_n) \ln \rho_{\text{dso}}(Q_n) dQ_n = \frac{k_{\text{B}}}{2} N_0 \ln \tilde{\sigma} + \text{const}, \quad (\Pi 13c)$$

$$\omega^2 = N_0\tilde{\omega}^2, \ \gamma = N_0\tilde{\gamma}, \ \Gamma = N_0\tilde{\Gamma}, \ N_0V_0 = N_0 \sum_{n'} V_{nn'} N_0 V_0 \equiv N_0 V_0(e_1, e_2) = \nu_0(1 + L_2e_1 + L_3e_2).$$

$$\tilde{J}(q_a) = \sum_{\Delta\mathbf{R}} \tilde{J}(|\Delta\mathbf{R}_{nn'}^{kk'}|)\cos(\mathbf{q}\Delta\mathbf{R}_{nn'}^{kk'}) \approx \sum_{i=0}^{2} \sum_{\Delta\mathbf{R}_i} \tilde{J}(|\Delta\mathbf{R}_i|)\cos(\mathbf{q}\Delta\mathbf{R}_i) = \tilde{J}_0 + \tilde{J}_1\cos(\Psi) + \tilde{J}_2\cos(2\Psi), \quad (\Pi 14)$$

$$\tilde{J}(|\Delta\mathbf{R}_{nn'}^{kk'}|) = \tilde{J}_{nn'}^{kk'} = J(|\Delta\mathbf{R}_{nn'}^{kk'}|) + L(|\Delta\mathbf{R}_{nn'}^{kk'}|)Q_0^2$$

Effective integrals of exchange interaction between magnetically active atoms at distance $|\Delta\mathbf{R}_{nn'}^{kk'}|$,

$$\Psi = q_a c_{\text{hex}}/2, \quad 2\Psi = q_a c_{\text{hex}},$$

c_{hex} — hexagonal lattice constants along axis $0z$.

$$\tilde{J}(0) \equiv \tilde{J}(q_a = 0) \equiv \tilde{J}(\Psi = 0) = \tilde{J}_0 + \tilde{J}_1 + \tilde{J}_2, \quad (\Pi 15a)$$

$$\tilde{J}_1 = \sum_{\Delta\mathbf{R}_i} \left[J(|\Delta\mathbf{R}_i|) + L(|\Delta\mathbf{R}_i|)Q_0^2 \right] = J_i + L_1Q_0^2, \quad (\Pi 15b)$$

$\Delta\mathbf{R}_i = [\Delta R_x, \Delta R_y, ic_{\text{hex}}/2]$, $J_i \equiv J_i(Q_0)$, in approximation of closest neighbors $\sqrt{\Delta R_x^2 + \Delta R_x^2} \approx a_{\text{hex}}$.

From minimum condition $\tilde{\Omega}_s + \tilde{\Omega}_Q \equiv \tilde{\Omega}$ relative to h we obtain

$$h = 2s\,y\left[\tilde{J}(q_a)\sin^2(\vartheta) + \tilde{J}(0)\cos^2(\vartheta)\right] + 2\mu_0 H_0\cos(\vartheta). \quad (\Pi 16)$$

Then full TP of $\Omega = \tilde{\Omega} + \Omega_e$ system considering (A16) can be written as

$$\Omega = ah_m(Q_0, e_1)y^2 - k_{\text{B}}NT\ln z(X) + U(Q_0, \tilde{\sigma}) - T\frac{k_{\text{B}}}{2}N_0\ln\tilde{\sigma} + \Omega_e, \quad (\Pi 17)$$

$$h_m = s^2\left[\tilde{J}(q_a)\sin^2(\vartheta) + \tilde{J}(0)\cos^2(\vartheta)\right],$$

$$a = N\tilde{J}(q = Q_0 = e_1 = 0)s^2 = (3/2)s^2a_3T_0/s(s+1),$$

$$a_2 = N_0k_{\text{B}} = 2(1-x)a_3, \quad a_3 = Nk_{\text{B}}.$$

Equilibrium dependences of magnetic, structural and elastic model characteristics can be obtained from the equations

$$\partial J(q_a)/\partial\Psi = 0, \quad \partial\Omega/\partial\vartheta = 0, \quad \partial\Omega/\partial\sigma = 0,$$

$$\partial\Omega/\partial e_1 = 0, \quad \partial\Omega/\partial e_2 = 0, \quad (\Pi 18)$$

$$\partial\Omega/\partial y = 0, \quad \partial\Omega/\partial Q_0 = 0. \quad (\Pi 19)$$

The first of equations (A18) leads to the condition of existence of helimagnetic structure at $\mathbf{H}_0 = 0$. which at $\tilde{J}(Q_0, e_1) = -4\delta\tilde{J}_2(Q_0, e_1) > 0$ and $\tilde{J}_2(Q_0, e_1) < 0$ has the form

$$\cos\Psi = \begin{cases} \delta(Q_0) & \text{by} \quad |\delta(Q_0)| < 1, \\ 1 & \text{otherwise.} \end{cases} \quad (\Pi 20)$$

In this case, the competing states will be only the helicoidal

$$(\cos\Psi = \tilde{J}_1(Q_0, e_1)/4|\tilde{J}_2(Q_0, e_1)| = \delta < 1)$$

with a higher value of $\tilde{J}(q_a)$

$$(\tilde{J}(q_a) = \tilde{J}_0(Q_0, e_1) + (2\delta^2 + 1)|\tilde{J}_2(Q_0, e_1)|)$$

and ferromagnetic ($\Psi = 0$) with lower value of $\tilde{J}(0)$

$$\left(J(0) = \tilde{J}_0(Q_0, e_1) + (4\delta - 1)|\tilde{J}_2(Q_0, e_1)|\right)$$

because at $\delta < 1$

$$\Delta\tilde{J}(q_a) \equiv \tilde{J}(q_a) - \tilde{J}(0) = 2(\delta - 1)^2|\tilde{J}_2(Q_0, e_1)| > 0.$$

The second equation (A18) with $\mathbf{H}_0 = [0, 0, H_0] > 0$ leads to the condition

$$\cos\vartheta = \begin{cases} \dfrac{2H_0\mu_{\text{B}}}{\left(J(q_a) - J(0)\right)y} & \text{by} \quad |\delta(Q_0)| < 1 \\ & \text{and} \quad 0 < \dfrac{2H_0\mu_{\text{B}}}{\left(J(q_a) - J(0)\right)y} < 1, \\ 1 \quad \text{otherwise.} \end{cases} \quad (\Pi 21)$$

Moreover, if we assume that HM structure is limited to the region of existence of the orthorhombic phase, then $\delta(Q_0)$ can be represented by the relation

$$\delta(Q_0) = 1 - AQ_0^2 + BQ_0^4. \qquad (\Pi 22)$$

The coefficients A and B vary the spontaneous and field characteristics of the HM structure.

The equilibrium values of the dispersion $\tilde{\sigma}$ of volumetric deformations e_1 and orthorhombic distortions e_2, satisfying the last 3 equations (A18) have the form

$$\tilde{\sigma} = \tilde{\sigma}(Q_0, T), \qquad (\Pi 23a)$$

$$e_1 = e_1(Q_0, y, T), \qquad (\Pi 23b)$$

$$e_2 \equiv e_2(Q_0) = \frac{L_3}{2} Q_0^2 \kappa_2. \qquad (\Pi 23c)$$

References

[1] J.S. Niziol, A. Zieba, R. Zach, M. Baj, L. Dmowski. JMMM **38**, 205 (1983).

[2] I.F. Gribanov, A.V. Golovchan, V.D. Zaporozhets, V.I. Kamenev, L.D. Klishchenko, V.V. Koledov, V.I. Mityuk, A.P. Sivachenko. FTVD **28**, *3*, 13 (2018). (in Russian)

[3] Yu.S. Koshkid'ko, E.T. Dilmieva, J. Cwik, K. Rogacki, A.P. Kamantsev, V.V. Koledov, A.V. Mashirov, V.G. Shavrov, V.I. Valkov, A.V. Golovchan, A.P. Sivachenko, S.N. Shevyrtalov, V.V. Rodionova, V. Sampath. J. Alloys Compd. **798**, 810 (2019).

[4] V.I. Val'kov, V.I. Kamenev, V.I. Mityuk, I.F. Gribanov, A.V. Golovchan, T.Yu. Delikatnaya. FTT **59**, 266 (2017). (in Russian).

[5] V.I. Val'kov, A.V. Golovchan, V.V. Koledov, V.I. Mityuk, I.F. Gribanov, V.D. Zaporozhets, B.M. Todris, T.S. Sivachenko. FTVD **29**, *3*, 5 (2019). (in Russian)

[6] V.I. Val'kov, V.I. Kamenev, A.V. Golovchan, I.F. Gribanov, V.V. Koledov, V.G. Shavrov, V.I. Mityuk, P. Duda. FTT **63**, *5*, 628 (2021). (in Russian)

[7] B. Penca, A. Hoserb, S. Barana, A. Szytułaa. Phase Transitions **91**, *2*, 118 (2018).

[8] A. Szytuła, S. Baran, T. Jaworska-Goła, M. Marzec, A. Deptuch, Yu. Tyvanchuk, B. Penc, A. Hoser, A. Sivachenko, V. Val'kov, V. Dyakonov, H. Szymczak. J. Alloys Comp. **726**, 978, (2017).

[9] D. Mattis. Teoriya magnetizma. Mir, M., (1967), 4097 s. (in Russian).

[10] L.D. Landau, E.M. Lifshits. Teoriya uprugosti. Nauka, M. (1987). 245 s. (in Russian)

[11] I.F. Gribanov, V.V. Burkhovetsky, V.I. Valkov, A.V. Golochan, V.D. Zaporozhets, V.I. Kamenev, T.S. Sivachenko. FTVD **30**, *1*, 83 (2020). (in Russian)

[12] V.I. Valkov, A.V. Golovchan, I.F. Gribanov, E.P. Andreichenko, O.E. Kovalev, V.I. Mityuk, A.V. Mashirov. V sb.: Dni kaloriki v Dagestane: funktsional'nye materialy i ikh prilozheniya. (27–May 31, 2023), Derbent S. 43–454.

[13] B. Zeks, R. Blinc. Soft modes in ferroelectrics and antiferroelectrics. Series of Monographs on Selected Topics in Solid State Physics. Elsevier, N.Y. (1974). V. 13. 398 p.

Translated by I.Mazurov